Biomaterials 276 (2021) 121026

Contents lists available at ScienceDirect

Biomaterials

journal homepage: www.elsevier.com/locate/biomaterials

Skin-inspired gelatin-based flexible bio-electronic hydrogel for wound healing promotion and motion sensing

Manhui Zheng [a], Xuechuan Wang [a,**], Ouyang Yue [a], Mengdi Hou [a], Huijie Zhang [a], Sebastian Beyer [b], Anna Maria Blocki [b], Qin Wang [c,d], Guidong Gong [c], Xinhua Liu [a,***], Junling Guo [c,e,f,*]

[a] College of Bioresources Chemical and Materials Engineering, Institute of Biomass & Functional Materials, Shaanxi University of Science &Technology, Xi'an, 710021, China
[b] Institute for Tissue Engineering and Regenerative Medicine & Department of Biomedical Engineering, Chinese University of Hong Kong, Hong Kong, SAR, China
[c] BMI Center for Biomass Materials and Nanointerfaces, School of Biomass Science and Engineering, Sichuan University, Chengdu, Sichuan, 610065, China
[d] School of Pharmacy, Southwest University for Nationalities, Chengdu, Sichuan, 610051, China
[e] John A. Paulson School of Engineering and Applied Sciences, Harvard University, Boston, MA, 02115, United States
[f] State Key Laboratory of Polymer Materials Engineering, Sichuan University, Chengdu, Sichuan, 610065, China

ARTICLE INFO

Keywords:
Gelatin hydrogels
FLexible bio-electronics
Electric stimulation
Motion sensor
Wound healing

ABSTRACT

Next generation tissue-engineered skin scaffolds promise to provide sensory restoration through electrical stimulation in addition to effectively rebuilding and repairing skin. The integration of real-time monitoring of the injury motion activities can fundamentally improve the therapeutic efficacy by providing detailed data to guide the clinical practice. Herein, a mechanically-flexible, electroactive, and self-healable hydrogels (MESGel) was engineered for the combinational function of electrically-stimulated accelerated wound healing and motion sensing. MESGel shows outstanding biocompatibility and multifunctional therapeutic properties including flexibility, self-healing characteristics, biodegradability, and bioelectroactivity. Moreover, MESGel shows its potential of being a novel flexible electronic skin sensor to record the injury motion activities. Comprehensive *in vitro* and *in vivo* experiments prove that MESGel can facilitate effective electrical stimulation, actively promoting proliferation in Chinese hamster lung epithelial cells and therefore can accelerate favorable epithelial biology during skin wound healing, demonstrating an effective therapeutic strategy for a full-thickness skin defect model and leading to new-type flexible bioelectronics.

1. Introduction

Skin functions as a protective and sensing interface while it can be damaged by burning, mechanical injuries, etc., for which healing can be impaired by peripheral vascular disease, immune dysfunction or metabolic diseases. Particularly, full thickness dermal wounds exceeding a critical size cannot be always self-healed [1,2]. Despite the great efforts to the development of wound dressing materials and therapies [3], effective wound healing remains a great therapeutic challenge, especially for the large-area and complex tissue damages [4,5]. Tissue-engineered skin can be obtained by seeding cells within and on a three-dimensional scaffold, providing a promising therapeutic method to rebuild and repair the skin barrier. Due to their advantageous capability to absorb wound exudates and preserve moisture, hydrogels can be used both as wound dressings and tissue scaffolds [6–9]. Self-healing hydrogels have aroused widespread attention in diverse biomedical applications due to their capability to restore their initial structure and mimic the complex regeneration process of natural skin, owing to their dynamic and reversible linkages in the hydrogel networks [10]. Moreover, since the scaffold acts as a biomimetic extracellular matrix (ECM) to promote cell infiltration, proliferation, differentiation, and *de novo* tissue formation, it should resemble inevitable significant characteristics

* Corresponding author. BMI Center for Biomass Materials and Nanointerfaces, School of Biomass Science and Engineering, Sichuan University, Chengdu, Sichuan, 610065, China.
** Corresponding author.
*** Corresponding author.
E-mail addresses: wxc-mail@163.com (X. Wang), liuxinhua@sust.edu.cn (X. Liu), junling.guo@scu.edu.cn, junlingguo@g.harvard.edu (J. Guo).

https://doi.org/10.1016/j.biomaterials.2021.121026
Received 5 February 2021; Received in revised form 27 June 2021; Accepted 12 July 2021
Available online 15 July 2021

of the natural ECM, including the chemical constitution and physical structure [11].

Gelatin is a denatured collagen that mimics components of the native ECM in terms of primary structure and chemical composition [12–14]. It has a wide applications for tissue engineering and regeneration on account of Arg-Gly-Asp (RGD) peptides, tissue adhesiveness, and thermo-sensitivity [15,16]. RGD sequence can not only increase the cellular bioactivity of scaffolds, but also promote cell adhesion and migration [17,18]. Recently, there have been elegant designs and engineering of gelatin self-healing hydrogel scaffolds to surmount traditional drawbacks (e.g. tissue adhesiveness, biocompatibility and deficient mechanical properties, etc.) [19,20]. However, therein still lies a common limitation among them: mechanical properties and versatility. Therefore, the rational design and engineering of gelatin-derived self-healing hydrogels, in this regard, show a great promise to overcome these issues due to their dynamic crosslinked molecular structure, outstanding biocompatibility, smart response, promotion of angiogenesis.

Skin is sensitive to electrical signals with conductivity values of 2.6 to 1×10^{-4} mS cm^{-1} varying among different parts of body [21]. Since 1960s, researchers have been studying the electrical stimulation therapy and its effect on wound repairing [22–25]. Importantly, it has been proved that the endogenous electric field has a positive effect on wound healing; therefore, it is crucial to compensate the endogenous electric field of a lesion to accelerate the recovery of its structure and function through an external electrical stimulation applied to imitate natural electric current in cutaneous wounds [26,27]. Electrical stimulation can be divided into two types: bidirectional current and unidirectional current, for example, including the direct current (DC) and unidirectional pulse current (PC) [21]. Unidirectional current can be used for simulate endogenous electric field due to its property of constant polarity and unbalanced charge. Although, bidirectional current has fewer adverse reactions and less invasive, DC is more effective in enhancing tissue perfusion and rate of wound area reduction [28]. Either unidirectional current or bidirectional current has the similar effects on wound healing. Moreover, we specifically chose the electric field intensity of 100 mV/mm and frequency of 25 Hz for the DC power source based on the following comparison table (Table S1). This electrical stimulation can mainly promote the proliferation of fibroblasts, the production of collagen, and growth factors. Electrical stimulation has been widely used as a physical therapy to accelerate tissue healing and functional recovery, owing to the introduction of the electrical stimulation and transduction of electrobiological signals [29–31]. This combinational electroactivity can lead to the promotion of cell proliferation, growth factor secretion, ECM synthesis and assembly, and revascularization. Nevertheless, there is still a gap for the application of electrical stimulation in the effective repair of severe tissue damages, due to its ineffective transduction into deeper tissues [32]. The electrical stimulation signal can be strengthened by the proper design and use of electroactive materials, mainly owing to the effective transmission to the defective tissue, leading to enhancement of tissue recovery [33]. Specifically, the enhanced electrical stimulation through direct current can govern the cellular activities by activating transmembrane channels [34], increasing intracellular Ca^{2+} concentration [35–37], thus leading to better therapeutic outcomes of wound healing in a simple and cost-effective way.

From a fundamental perspective, the major scientific challenge for electroactive materials resides within the engineering of proper conductivity of the scaffolds, while not compromising the hydrogels' physicochemical properties, such as toughness, stretchability, and biocompatibility. The development of a new-type of "smart" viable electroactive biomaterials should be capable of creating an ideal electronics-skin interface to effectively transport the electrochemical and electrobiological signals to the cells within the affected tissue, generating a range of therapeutic responses, including cellular proliferation and differentiation of electrical signal sensitive cells (for example, fibroblasts, nerve, bone, and muscle cell) [38,39]. Additionally, imparting the functionality of motion tracking at the wound areas has shown potential to benefit the wound treatment process, by monitoring the epidermal changes real-time. Accelerated skin wound healing through the integration of electronics-based motion activity tracking capability also illustrates its great potential for point-of-care treatment [40,41]. Conducting polymers have been suggested as promising material candidates in tissue engineering restoration, endowing scaffolds with electrical, antibacterial properties, and controlled release of bioactive agents and drugs [42]. These advantageous properties allow an establishment of suitable bio-nano interfaces to transmit/receive the electrical stimulation to/from the cellular levels of wound tissues [43]. Elegant advances has been achieved through the use of various conducting polymers, including polypyrrole (PPy) [44], polyaniline (PANI) [45], polythiophene (PTh) [46], and PEDOT:PSS [47–51], while the employment of biologically-originated polymers provides an ideal platform for the engineering of a bio-inspired multifunctional 3D-scaffold for tissue-engineered skin by taking advantage of the bioactivity and biocompatibility properties.

Herein, we developed a bioinspired gelatin-based smart 3D-scaffold through the integrative crosslinking strategy of N-(3-Dimethylaminopropyl)-N′-ethylcarbodiimide hydrochloride (EDC) to incorporate the functional building blocks of water-dispersible conducting polymer complex, PEDOT:PSS, and MWCNTs-COOH (Fig. 1A). These gelatin-based smart 3D-scaffold, possessing the desirable properties of mechanical flexibility, electroactivity, and self-healing, (termed as 'MESGel'), were engineered by a simple and facile "one-pot" preparation strategy through physical doping and chemical crosslinking. A range of molecular interactions among the components in MESGel provides an integrative crosslinking strategy to form a 3D-network in the bio-inspired hydrogel, which are conducive to the performance of multifunctional therapeutic properties. Moreover, with this multifunctionality design, MESGel considerably promotes wound healing through precise electrical stimulation and wearable motion sensing function at the wound injury area, leading to new-type flexible bioelectronics as the integration of real-time monitoring of injury motion activities. This next-generation function of MESGel can fundamentally improve the therapeutic efficacy by providing detailed data to guide the clinical practice. (Fig. 1B and C). In particular, the combination of electroactivity and bioelectronics in these materials effectively accelerates cell proliferation in a full-thickness skin defect model by the external electric field applied to the scaffolds, and simultaneously monitors the real-time movements of the human body. This work presents a new avenue for exploring more multifunctional hydrogels inspired by nature for biomedical applications.

2. Results and discussion

2.1. Design strategy and structural characterization of MESGel

Gelatin containing RGD sequence has adhesive domains and matrix metalloprotein (MMP) sensitive sites linked to cell binding and cell-mediated matrix degradation [52,53]. The PEDOT:PSS can be incorporated into the gelatin backbone to increases the electrical conductivity and flexibility of the hydrogel. After adopting the home-made MWCNTs-COOH, the electrical conductivity, mechanical properties and antibacterial ability can be further improved. Subsequently, the gelatin chains are crosslinked by EDC through amide bond formation, which further increased the mechanical properties of the hydrogel. A range of molecular interactions provides an integrative crosslinking strategy to the formation of the 3D-network of the bio-inspired hydrogel, including hydrogen bonds, electrostatic interactions, and aromatic π-π interactions [54–57]. MESGel can be used for skin regenerative scaffolds to promote wound healing under electrical stimulation (ES) (Fig. 1B) and simultaneously monitor the motion activities of the wound area (Fig. 1C).

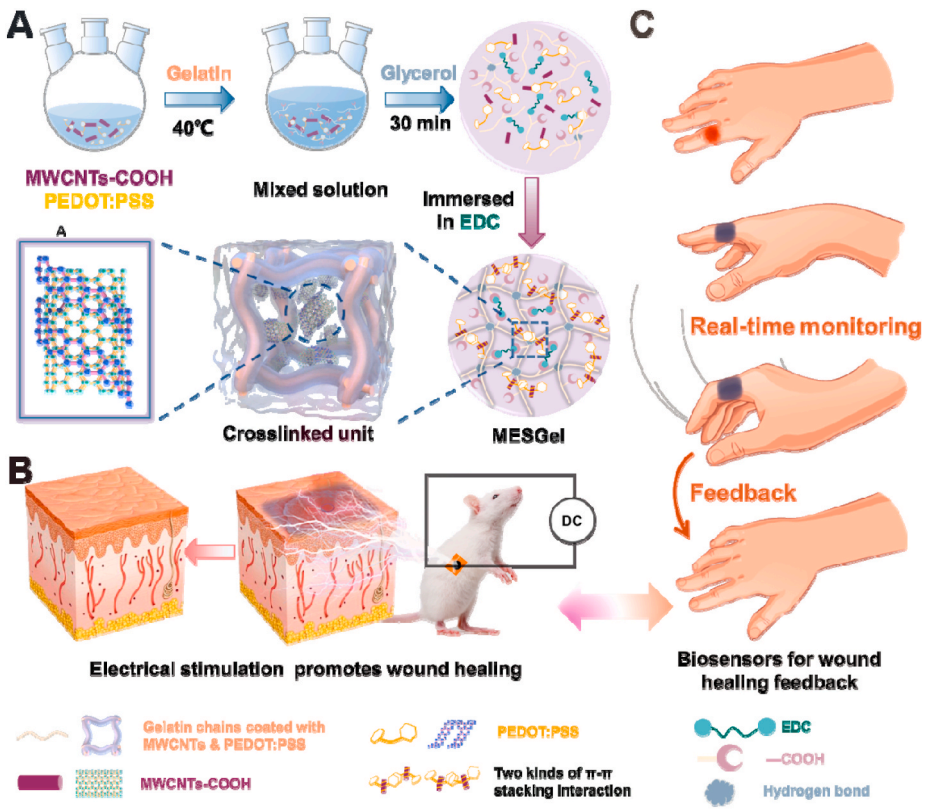

Fig. 1. Schematic illustration of the fabrication and application of multifunctional MESGel hydrogels. (A) Synthetic process of MESGel. (B) Electrical stimulation promotes wound healing. (C) Real-time monitoring and feedback of MESGel biosensors for wound healing.

Different types of hydrogels photographed were fabricated by adding MWCNTs-COOH or PEDOT:PSS or both, and crosslinked by EDC. A transparent gelatin hydrogel (GH) just cross-linked by EDC was used as the control group (Fig. 2A). The grayish hydrogel (GCH) was manufactured by gelatin and MWCNTs-COOH, and the light blue hydrogel (GPPH) was fabricated by gelatin and PEDOT:PSS. The novel MESGel was generated by combining gelatin, MWCNTs-COOH, and PEDOT:PSS (Fig. 2A (ii)). MESGels can be molded to many shapes (Fig. 2A (iii)), allowing for the easy and rapid control of applicable morphologies. According to the SEM analysis in Fig. 2B (i), the GH and MESGel hydrogels exhibited a porous 3D-nanostructure, which is the typical structure of gelatin-based hydrogels. The MESGel presented a smaller and more uniform pore diameter likely due to the cross-linking of EDC, the electrostatic adsorption between PEDOT:PSS, as well as the extensive hydrogen bonding between various substances (Fig. 2B (ii), (iii)). Besides, the microscopic distribution of PEDOT:PSS and MWCNTs-COOH in MESGel has been further observed. Scanning electron microscopy (SEM) images show the mixture of PEDOT:PSS (Fig. S9 A) and MWCNTs-COOH (Fig. S9 B) with flake-like structures. The SEM images also shows that the surface of MWCNTs-COOH is wrapped by PEDOT:PSS. The SEM image with higher magnification shows that the mixture of PEDOT:PSS and MWCNTs-COOH is uniformly distributed in the network structure of MESGel. To a certain extent, the water in the gap makes a continuous phase formed on the surface of gelatin molecular chain, which greatly improves the conductivity of MESGel.

Fig. 2C (i) showed the Raman spectra and mapping images and indicated a strong absorption peak at 1423 cm^{-1}, which is related to the symmetric stretching vibration of the $C_\alpha = C_\beta$ double bond on the aromatic ring of PEDOT. In addition, a prominent D-band peak appeared at 1262 cm^{-1} due to increased disorder in the sp^2 domains, and G-band peak appeared at 1518 cm^{-1} caused by a shorter range structure of the MWCNTs. The relative intensity (I_D/I_G) of the D- and G-band peaks can reveal the disorder degree and defect density of the sample. By comparison with the results in Fig. 2C (ii), it can be deduced that the MWCNTs-COOH in the MESGel were more ordered, probably due to that the MWCNTs-COOH were enwound by the PEDOT molecular chain, which is full of π-π stacking interactions. Furthermore, both the D- and G-band peaks red-shifted to low frequency ranges due to the hydrogen-bond interaction, as well as the extrusion force of PEDOT. Additionally, the Raman peak of PEDOT:PSS red-shifted from 1435 cm^{-1} to 1423 cm^{-1}, elucidating the chemical structure of PEDOT changing from benzoid to quinoid structure. In other words, the conductivity of PEDOT was improved due to the doping of MWCNTs-COOH.

2.2. Mechanical and self-healing properties of MESGel

As confirmed by the self-healing experiment, the MESGels has excellent self-healing properties mainly due to the abundant hydrogen bonds, electrostatic interactions, and aromatic π-π stacking interactions (Fig. 3A). It can be seen in Fig. 3B that the cut MESGels could be self-healed to 60% in 2 min and approximately 100% in 10 min, illustrating that MESGels possessed self-healing property. And this is in good agreement with the result of alternate step strain sweep test (Fig. 3E). The rheological properties of the MESGels was inspected by the detection of storage modulus (G′) and loss modulus (G"). The results of frequency-dependent oscillatory shear rheology at a constant strain of 1% of the four types of hydrogels (Fig. 3C) exhibited that G′ was dominant in the frequency range of 0.1–100. Among them, MESGels had the highest G′, indicating a higher strength.

Notably, the MESGel had transition from solid-to liquid-like state at higher strains (the intersection of G' and G" curves), exhibited a broad linear viscoelastic region and a great anti-shear ability. The molecular structure of MESGel was merely destroyed at strains over 40% (Fig. 3D), showing a wide processing range and shear-thinning behavior. A high strain (200%) was applied to break the entanglement network structure of the hydrogel molecular chains, followed by a low strain (10%) to

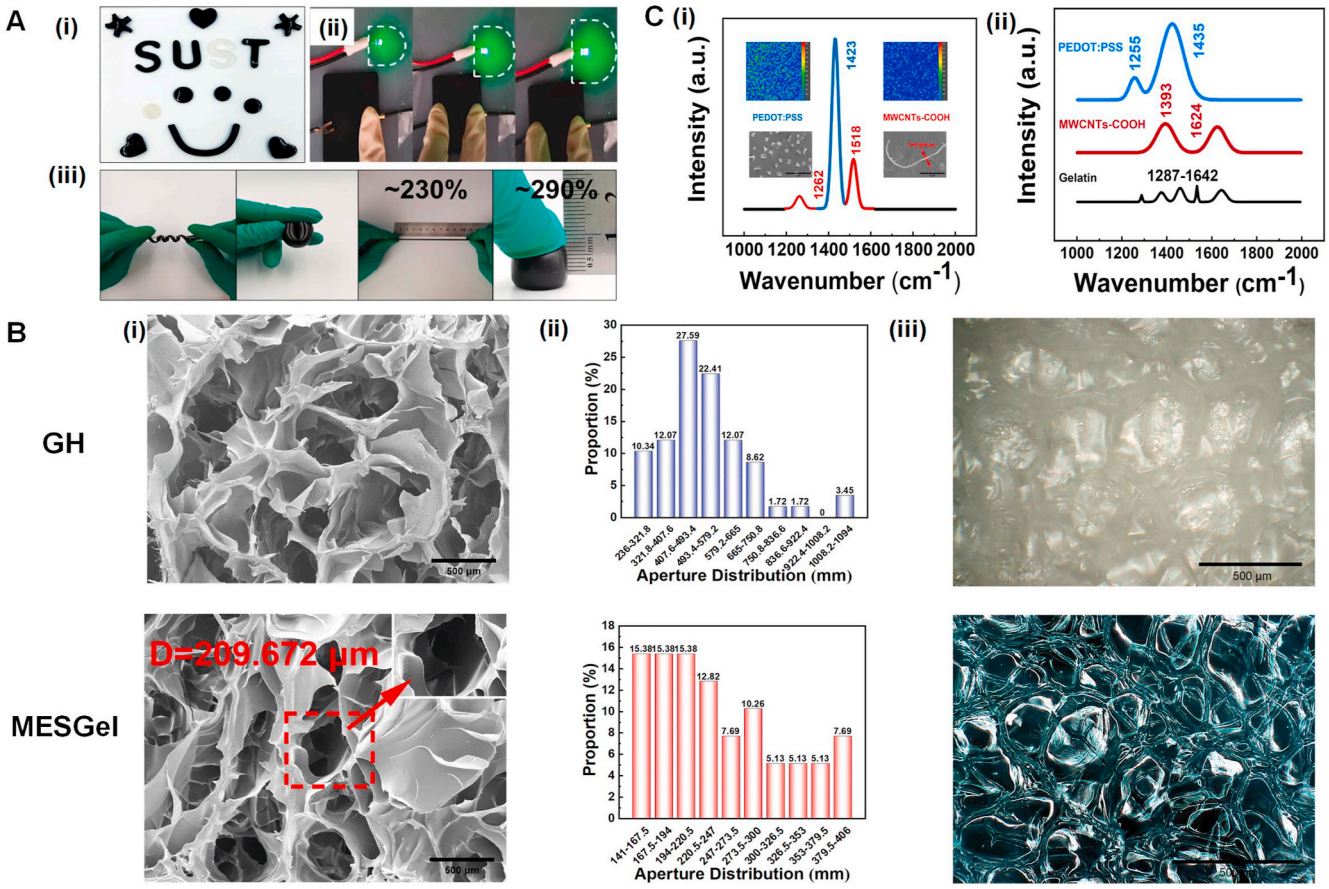

Fig. 2. Structural characterization of MESGel hydrogel and counterparts. (A) Photographs of "SUST" and "a smiley face" consisting of gelatin hydrogel (GH) and MESGel hydrogels (i); Experiment of MESGel hydrogel in a DIODE circuit under different applied pressure levels (ii); From left to right, the images showed the deflection, bending, stretching and compression properties of the MESGel hydrogel (iii). (B) SEM micrographs (i); aperture distribution (ii); and optical microscopy images (iii) of the GH and MESGel hydrogels. (C) Raman spectra and mapping images of PEDOT:PSS and MWCNTs-COOH of the MESGel hydrogel (i) and single PEDOT:PSS, MWCNTs-COOH, and gelatin (ii).

study the recovery property of the MESGel. Over three cycles of breaking and recovering, the broken internal structure of MESGel recovered fleetly and displayed a hydrogel-like behavior (Fig. 3E). This property is critical for scaffolds to repair the micro-cracks caused by tissue stress during cell proliferation.

The MESGel scaffold exhibited good mechanical properties, including both tensile (Fig. 3F) and compressive (Fig. 3G), compared to those of GH and GCH. This result was attributed to that the addition of MWCNTs-COOH and PEDOT:PSS enhanced the stiffness and toughness of the MESGel hydrogel scaffold. In addition, EDC links gelatin fibers 'hand in hand'. The MESGel hydrogel scaffold was able to withstand a tensile strain as high as 425% and a compressive strain as high as 71%. It should be mentioned that, after self-healing, the MESGel hydrogel scaffold was able to reach a tensile strain of 375% and a compressive strain of 65%, which benefits the service life of the scaffold to a certain extent.

The design of proper biodegradability rate of tissue engineered materials adapted to the natural tissue growth rate remains a great challenge. For instance, collagen derived materials are biomedical materials that can be absorbed by the human body. However, it has been reported that their excessively fast degradation rate (DR) in certain wound repairs cannot match the growth and repair rate of tissues, thus slower DR of collagen-derived materials are desired [58]. The *in vitro* degradation of the hydrogels was evaluated in PBS at 37 °C. The DR of the MESGel scaffold was the lowest (Fig. 3H) due to its more compact structure compared to that of the GH, GCH, and GPPH hydrogels, which can be also found in Fig. 2B. Combined with the insert part, the *in vitro* DR of MESGel (92.34%) is 4.5 times as high as *in vivo* full-thickness skin defect model DR (20.37%) in about three weeks. It may be caused by the warmer and moister degradability environment *in vitro* compared with on wound skin surface. The swelling ratio was measured to evaluate the swelling properties of the hydrogel. As depicted in Fig. 3I, after 24 h, the equilibrium swelling ratio of the hydrogels exceeded 4.5. It needs to be pointed out that the swelling ratio increased rapidly in the first five days. This is attributed to water molecules forming hydrogen bonds with the hydrophilic groups of the hydrogel components, thus forming a primary hydration water with a certain degree of relaxation and extension in the molecular chain. Subsequently a slower process took place, where hydrophobic groups might form bonds with water molecules to form the secondary hydration water until reaching the swelling equilibrium. Moreover, the trends of the *in vitro* DR of the four types of hydrogels were comparable.

The thermal denaturation temperature is a critically important for the application of biopolymer-based materials. Fig. 3J presents the differential scanning calorimetry (DSC) experiment results, where the thermal denaturation temperature (T_d) of the MESGel hydrogel scaffold increased by integrating PEDOT:PSS and MWCNTs-COOH as compared to GH, GCH, and GPPH hydrogels (MESGel > GPPH > GCH > GH). Generally, the added MWCNTs-COOH were adsorbed to the surface of the gelatin chains and impeded the generation of intermolecular hydrogen bonds. Nevertheless, the functionalized MWCNTs-COOH enwound by PEDOT strikingly enhanced the hydrogen bonds in the three-dimensional structure. This crisscrossing hydrogen bond network provided a more solid structural basis for the stability of the MESGel

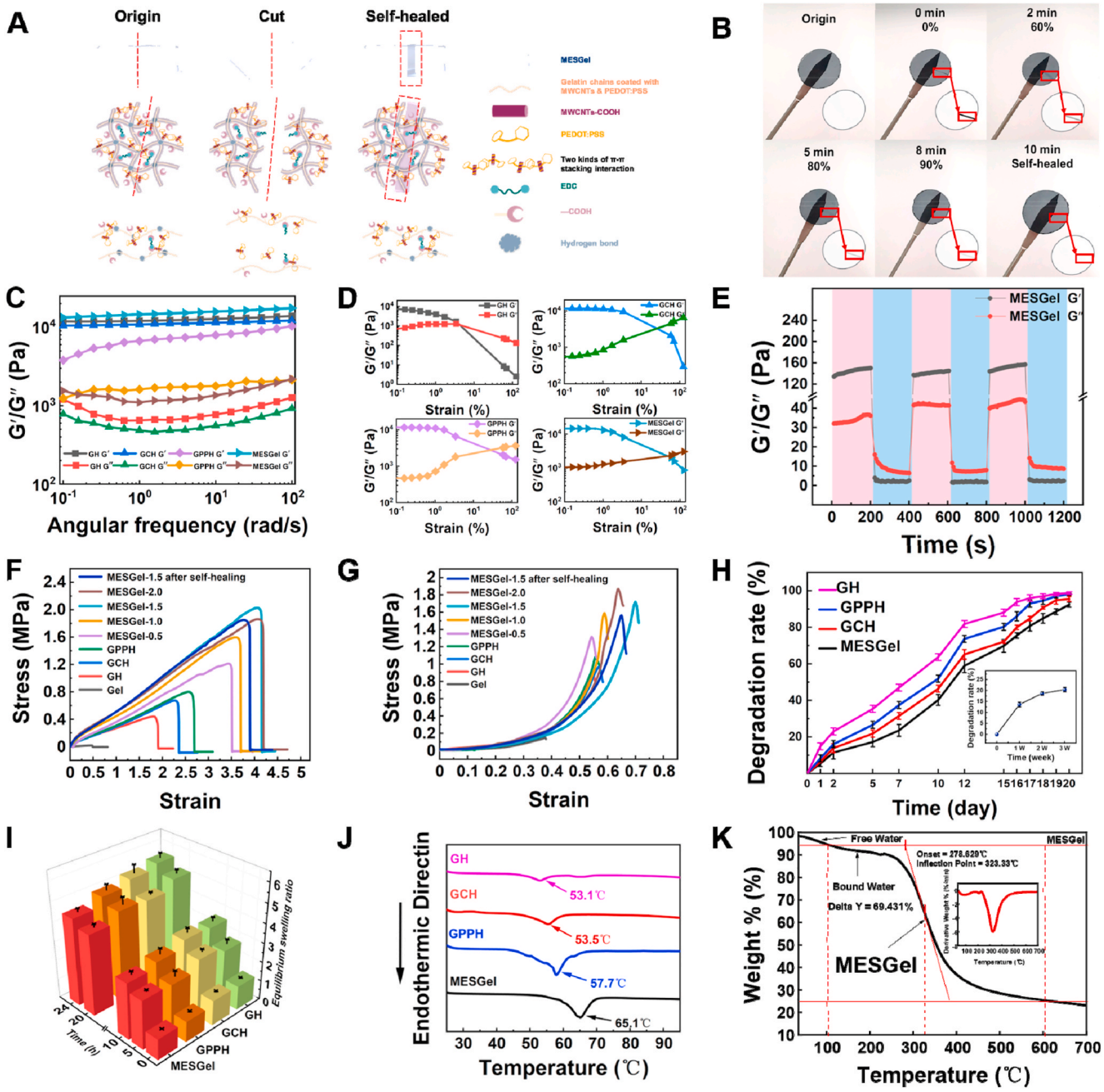

Fig. 3. Structural characterization and mechanical properties of MESGel hydrogel and counterparts. (A) Self-healing mechanism diagram of the MESGel hydrogel driven by the integrative crosslinking strategy. (B) Photos of the MESGel self-healing process. Frequency-dependent (C) and strain-dependent (D) oscillatory rheology results of composite hydrogels. (E) Alternate step strain sweep test results for the MESGel. Tensile (F) and compressive (G) stress-strain curves of different hydrogels. (H) *In vitro* degradation rate (DR) and *in vivo* full-thickness skin defect model DR (inset). Swelling behavior (I), and DSC curves (J) of composite hydrogels. (K) TG and DTG curves of the MESGel.

hydrogel scaffold. The measured T_d values were: MESGel (65.1 °C) > GPPH (57.7 °C) > GCH (53.5 °C) > GH (53.1 °C). According to the thermogravimetry (TG) and derivative thermogravimetry (DTG) curves (Fig. 3K), the thermal weightlessness process can be divided into four steps: (1) Between 0 and 100 °C, the free water is lost in proportion to thermal weightlessness. (2) Between 100 and 250 °C, a large amount of chemically combined water is vaporized with the breakage of hydrogen bonds. On the other hand, the uncomplete triple helical structure of gelatin continued to unwind thoroughly. (3) Between 250 and 600 °C, the natural structure of gelatin was totally thermally decomposed to obtain minimal peptides and amino acids. (4) Above 600 °C, the residual micro-molecules were carbonized with carbon deposit removal. The measure glass transition temperatures (Tg) were: MESGel (323.3 °C) > GPPH (296.9 °C) > GCH (294.8 °C) > GH (294.5 °C), matching exactly with the results of the DSC experiment. It can be concluded that the thermal stability of the MESGel scaffold was significantly improved due to the combination of PEDOT and MWCNTs-COOH.

2.3. *MESGel for the epidermal sensor*

The electroactivity of hydrogels is essential for the electrical stimulation to the tissue cells. Therefore, the engineering of suitable conductivity has been recognized as the key for the design and fabrication of e-skin sensors. Fig. 4A illustrates the fabrication process of e-skin strain

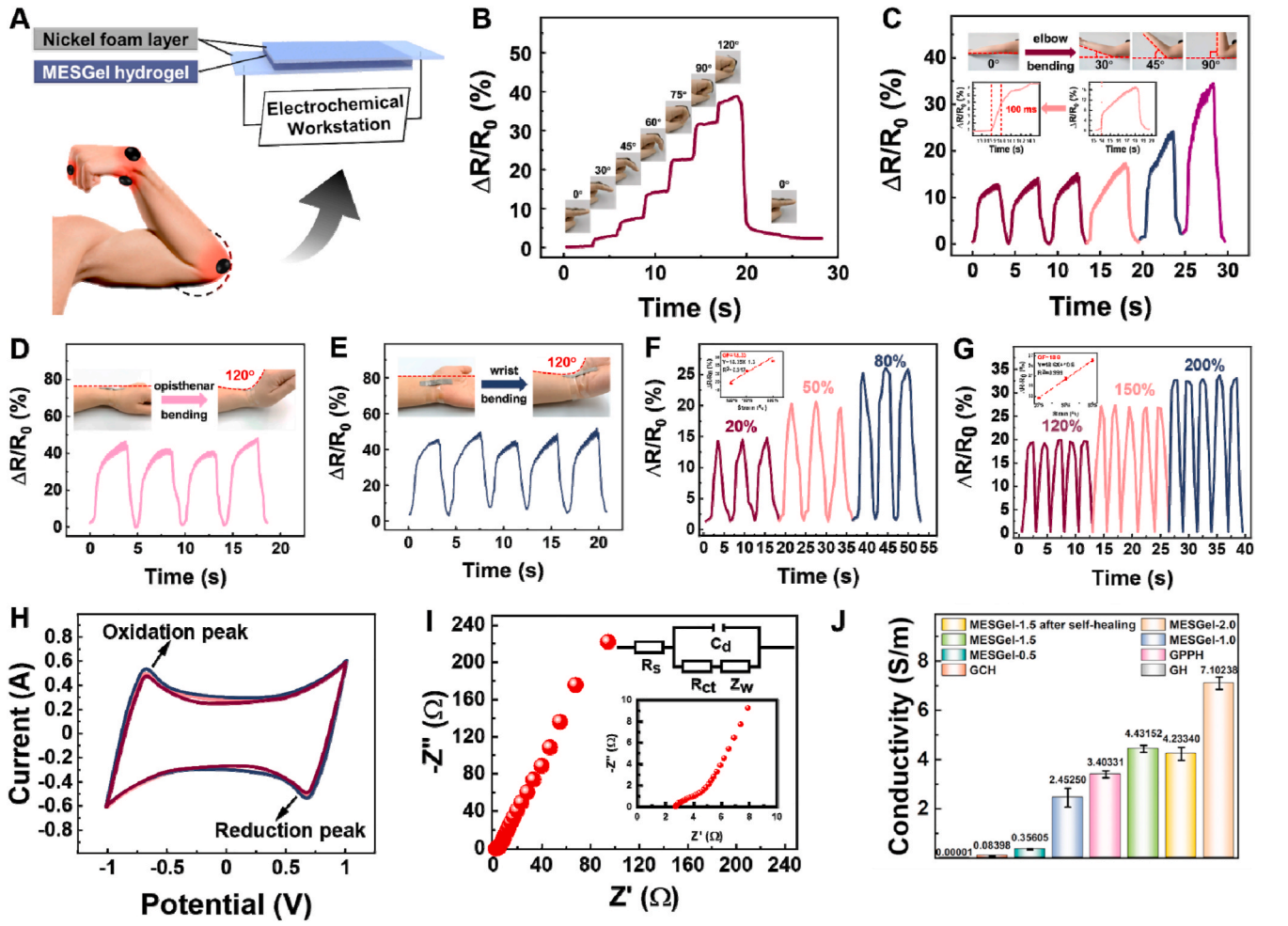

Fig. 4. Monitoring of joint movement and electrochemical properties of the MESGel hydrogel. (A) Schematic illustration of smart sensor construction and a human arm model. Related locations/joints, where movement could be monitored were marked with solid black circles. (B) Bending angle variation detection of finger, (C) arm flexion, (D) opisthenar, and (E) wrist. Relative resistance changes under different compressive (F) and tensile strains (G). (H) CV curve obtained at a scanning speed of 50 mV s^{-1}. (I) Impedance curve and equivalent circuit. (J) Conductivity of different hydrogels measured by the four-probe method.

sensors. This sandwich-like 3D-structure design not only provides protection but also ensures the good conductivity of the MESGel sensor. The variation sensitivity was detected by demonstrating the relative resistance ($\Delta R/R_0$ = *(D-value of resistance)/initial resistance* × *100%*) of a range of human joint motions including the monitoring of the knuckle (Fig. 4B), elbow (Fig. 4C), opisthenar (Fig. 4D), and wrist (Fig. 4E). According to Fig. 4B and C, the $\Delta R/R_0$ increased with the increase of the finger bending degree. There was a positive correlation between the two observations and the maximum values were 38.8% and 34.5%, respectively. It is worth mentioning that the response time (RT) was merely 100 ms, suggesting a high sensitivity for the epidermal sensor (Fig. 4C). During bending, the conjugated action of the PEDOT molecular chain is destroyed, and the molecular orbital provided for the charge carrier is reduced. Fig. 4D and E shows that when the wrist angle was up to 120°, the $\Delta R/R_0$ changed over 40%, which was identical to the conclusion obtained by Fig. 4B and C. The gauge factor (GF) can express the sensitivity of resistance to strain. When the compressive strain changed from 20% to 80%, the $\Delta R/R_0$ changed from 14.8% to 26.0% with a GF of 18.35 (Fig. 4F). Moreover, when the tensile strain changed from 120% to 200%, the $\Delta R/R_0$ changed from 19.6% to 33.7% with a GF of 18.6 (Fig. 4G). These results can be explained by the Poisson effect. The sensitivity of MESGel smart stretchable strain sensors was intrinsically limited because Poisson compression squeezed molecular chains together [59]. Therefore, the comprehensive experimental results exhibit that MESGel could serve as an e-skin sensor, which could be utilized for the real-time monitoring of the injury motion activities. However, it remains as a challenge to demonstrate the combinational performance of electrical stimulation wound healing and motion senor properties in a wound healing model yet. One of the key challenges is that the movements around the wound area lead to the unstable contact between the MESGel and skin. Further studies are currently ongoing to integrate an additional adhesive layer between the MESGel and skin to increase the stability of bio-material contact."

Fig. 4H displays the cyclic voltammetry (CV) experimental result within the −1.0 - 1.0 V range at a potential scanning speed of 50 mV/s. Analyzing the shape of the CV curve, it can be observed that there were two pairs of apparent oxidation and reduction peaks, and the characteristic peaks for the mutual conversion of PEDOT between different redox states, which is a unique pseudocapacitance characteristic of conductive polymeric materials. The Nyquist curve obtained from Electrochemical Impedance Spectroscopy (EIS) and the equivalent circuit diagram (inset) displayed in Fig. 4I show that the diffusion velocity was dominant during the disturbance process. In other words, the speed of charge transfer was very high, while the process of charged ions diffusion to the surface of the MESGel hydrogel electrode was very slow. Under this circumstance, the intercept of the Z′ axis was equal to the contact resistance (R_{ct}) plus the EIS film resistance (R_s), and Z′ was about 2.2 Ω. Therefore, it can be concluded that the MESGel has good capacitance properties and is a good candidate for super capacitor

applications. As it can be seen in Fig. 4J, the GH hydrogel was hardly conductive, while the MESGel conductivity increased to 7.1 S cm^{-1} when 2.0 mL of PEDOT:PSS were added. In addition, after self-healing, the MESGel was not far behind before cut attested in video S1, which signifying that it possessed excellent self-healing property and long cycle time. Due to its superior conductivity, it can be used as an e-skin sensor or supercapacitor.

Supplementary video related to this article can be found at https://doi.org/10.1016/j.biomaterials.2021.121026

To verify the cell proliferatory effect of MESGel scaffold under electrical stimulation, the MESGel scaffolds co-cultured with CHL cells were electrically stimulated according to the electrical stimulation cycle, as shown in Fig. 5A mentioned earlier. It can be seen in Fig. S2 that the CHL cells grew uniformly on the porous scaffold with conspicuous cell proliferation, and there were fewer dead cells on the MESGel + electrical stimulation for 5 days (Fig. 5F). Then, the cell morphology and proliferation ability were further evaluated by flow cytometry. According to the 2D scatter plot in Fig. S2, the side scatter (SSC) value of the MESGel + electrical stimulation was higher compared with MESGel, implying that the granularity of the cell was intact, and no difference in cell size since the forward scatter (FSC) value was also similar (Fig. 5G). The cell proliferation index (CPI) can be determined according to $CPI = S + G_2$. The CPI of the MESGel + electrical stimulation was 63.55 (day 1), 63.56 (day 3) and 63.7 (day 5), while that of the MESGel was 59.3 (day 1), 59.0 (day 3) and 59.1 (day 5). The higher CPI means most cells were in the DNA replication phase, entering the G_2 phase, and gradually entering the mitotic phase (Fig. 5D). In other words, electrical stimulation had a prominent positive effect on CHL cell proliferation.

2.4. Biocompatibility and electroactivity of MESGel

Methyl thiazolyl tetrazolium (MTT) assays and co-culturing assays with live/dead cell fluorescence staining recorded by laser scanning confocal microscopy (LSCM) were employed simultaneously to demonstrate the biocompatibility of the MESGel. As shown in Fig. 5A, a home-made electric stimulator was designed to apply ES. In the design, holes with a diameter of 0.5 cm were drilled through at both tops of each hole in a 12-well plate, so that the holes can be connected with each other, ensuring the formation of an electrical stimulation circuit. The contact of the AgCl electrodes with the culture medium was prevented by using Agar salt-bridges. As shown in Fig. 5B, the GH and MESGel hydrogels showed neglected toxicity compared with saline (NS), and according to the MTT assays, the cell viability exceeded 111.3% after 5 days in all cases (Fig. 5C). Moreover, fluorescence images of Chinese hamster lung cells (CHL) cultured on the MESGel scaffold at 37 °C at different time intervals are shown in Fig. S1. Almost no dead cells were found after 5 days of cocultivation (Living cells showed green fluorescence, in comparison, dead cells showed red fluorescence), indicating the high biocompatibility of MESGel (Fig. 5E).

2.5. Electrical stimulation of MESGel for full-thickness skin wound healing

The full-thickness skin defect model on SPF rats was used to estimate the induction and promotion of tissue healing. An external electrical stimulation powered by a DC supply was applied on MESGel hydrogel scaffolds (Fig. 6A). The macroscopic appearance of the wounds treated by different therapies on day 0, 3, 7 and 10 was provided in Fig. 6B. All

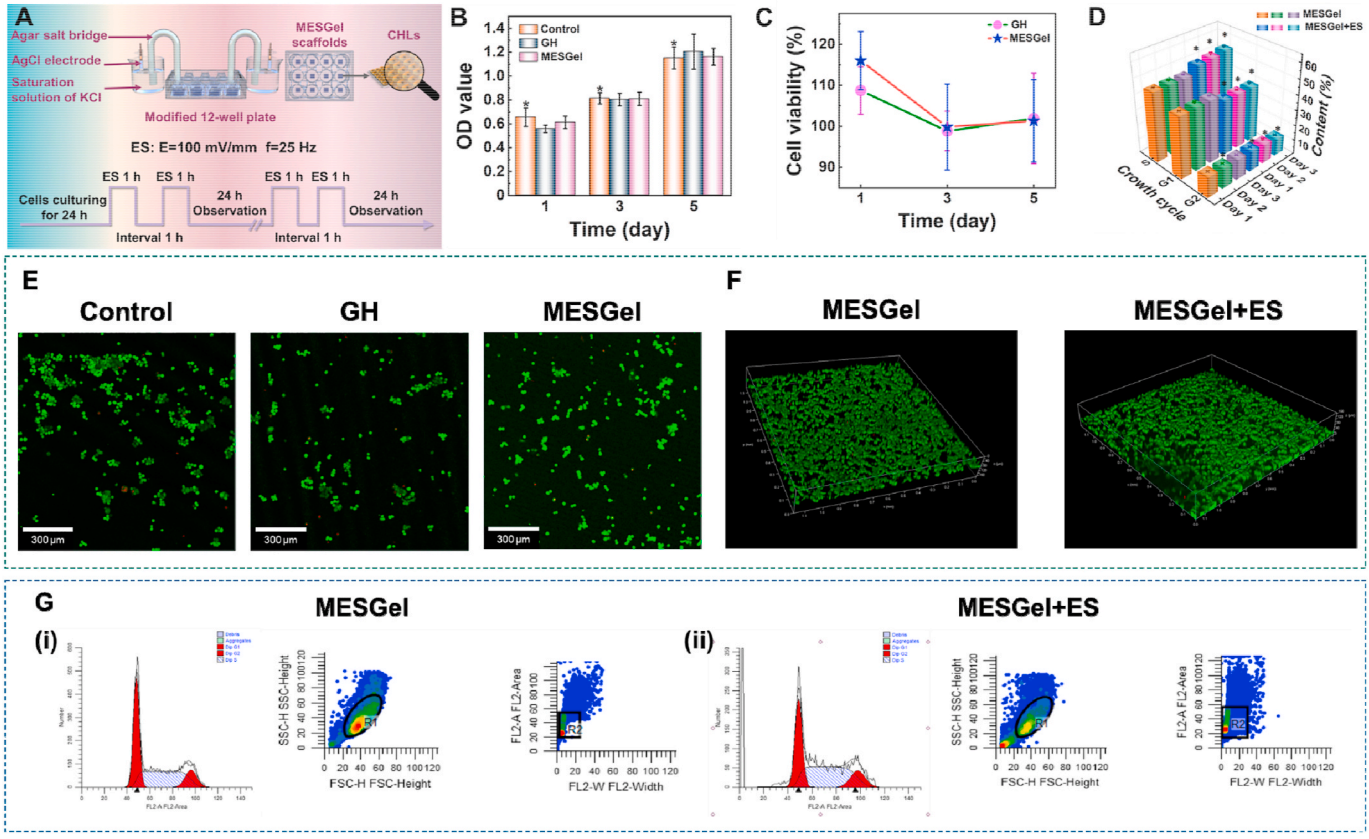

Fig. 5. Cell viability and multiscale morphology of MESGel scaffold. (A) Schematic of the experimental configuration and electrical stimulation cycle sequence applied to the MESGel. (B) Optical density at 450 nm (OD) values and (C) cell viability of the Chinese hamster lung cells (CHL) evaluated by MTT assays. (D) and (G) Flow cytometry results of the MESGel and MESGel + electrical stimulation. (E) LSCM images of Live/Dead staining and (F) co-culturing on the MESGel + electrical stimulation for 5 days. Scale bar: 300 μm. Data are depicted as mean ± SD (n = 6), and analyzed by one-way ANOVA with Tukey's multiple comparison test compared to NS group. The level of significance was set at *p < 0.05.

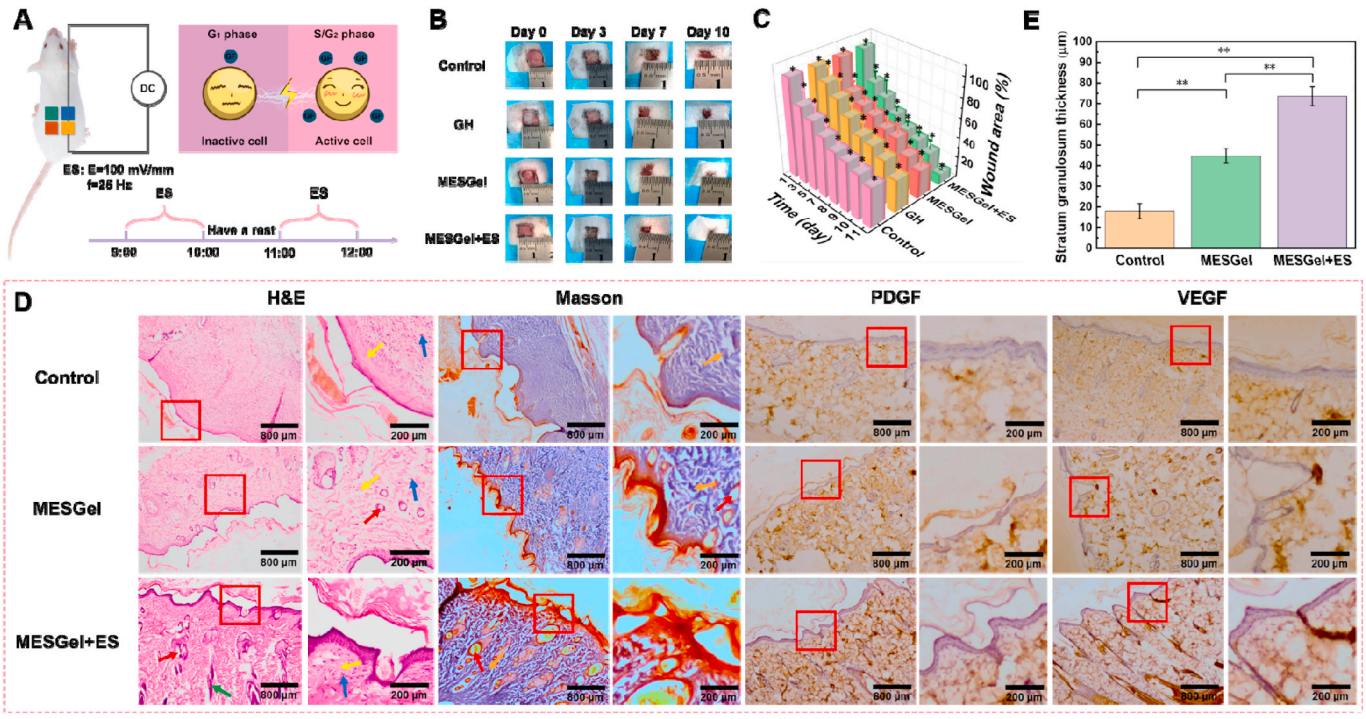

Fig. 6. Electrostimulation of SPF rats with full-thickness skin loss wounds. (A) Schematic of the *in vivo* skin wound treatment experiments. (B) Photographs of the differently-treated wounds on day 0, 3, 7 and 10. (C) The wound area (%) decreased within 10 days under the four treatments. (D) H&E staining, Masson staining and immunohistochemical staining of PDGF and VEGF in the wound area on day 20. Blood vessel (red arrow), fibroblast (yellow arrow), neutrophil (blue arrow), hair follicle (green arrow), collagen deposition (orange arrow), PDGF (brown-stained area) and VEGF (brown-stained area). (E) Stratum granulosum thickness of in the wound area on day 20. Data are depicted as mean ± SD (n = 6), and analyzed by one-way ANOVA with Tukey's multiple comparison test compared to NS group. The level of significance was set at *p < 0.05. (For interpretation of the references to colour in this figure legend, the reader is referred to the Web version of this article.)

wound areas decreased over time albeit at different rates: MESGel + electrical stimulation group > MESGel group > GH group > NS group. Another interesting finding was that, at any time point, the wounds treated with the MESGel + electrical stimulation had the smallest wound area among all groups, with a wound closure rate higher than 90% after 10 days of treatment, as depicted in Fig. 6C. It could be summarized that both the electroactive MESGel hydrogel scaffolds and electrical stimulation had the effect of promoting wound healing.

To further assess the capability of the MESGel and MESGel + electrical stimulation to promote healing, tissue sections of the wound on were analyzed by H&E and Masson staining and immunohistochemical staining of platelet-derived growth factor (PDGF and VEGF) on day 7, 14, and 20. Fig. 6D displayed these results on day 20 and more information can be found in Fig. S3~S6. The different expression strength of blood vessel (red arrow), fibroblast (yellow arrow), neutrophil (blue arrow), hair follicle (green arrow) and collagen deposition (orange arrow) in wound area are marked and highlighted in Fig. 6D. In control group, a basic structure of epithelium and dermis was formed with mild inflammatory reaction while hardly forming and depositing of collagen, new hair follicles and blood vessels were found. On the contrary, wounds treated with the MESGel scaffolds exhibited incomplete loose epithelium and dermis with fewer inflammatory neutrophils, formed hair follicles and blood vessels, indicating that the MESGel groups improved wound healing promotion. Particularly, the abundant regenerated hair follicles and blood vessels, a thicker new epidermal layer and a defined thicker tissue structure were distinctly observed in the wounds treated by the MESGel + electrical stimulation scaffolds, indicating a superior wound repair effect, including improvement of connective tissue remodeling and re-epithelization process.

The area and density of defined collagen fibers can reflect the formation of *de novo* tissue and the degree of healing to a certain extent. The wound healing process is closely related to the accumulation of collagen fibers, fibroblasts, and growth factors (GFs). After 20 days, depositional collagen (blue-stained area) appeared with various extent in three groups (Fig. 6D). Notably, the MESGel + electrical stimulation treatment had the highest collagen density and more organized fibrous structures, which further demonstrated its strong wound healing effect. Membrane channels, proliferation, migration of cells in wound area are regulated by GFs. PDGF acts as mitogen that can stimulate fibroblasts, glial cells, smooth muscle cells and other cells stagnanted in the G_0/G_1 phase to enter the division and proliferation cycle. Meanwhile, VEGF can promote vascular permeability increase, extracellular matrix degeneration, vascular endothelial cell migration, proliferation and angiogenesis. In this study, analysis of PDGF and VEGF expression was performed by immunohistochemistry. As shown in Fig. 6D, the expression of PDGF and VEGF (brown-stained area) in MESGel and MESGel + electrical stimulation was much higher than that in the control group, illustrating that electrical stimulation was able to promote wound recovery by enhancing the PDGF and VEGF expression. Consequently, the fibroblasts and keratinocytes proliferation, granulation tissues formation and re-epithelialization processes were accelerated, which were also consistent with the H&E and Masson trichrome staining results. In addition, the thickness of the stratum granulosum of tissue sections on healed wound area has been added in Fig. 6E. The variation rule of stratum granulosum thickness is as follows: MESGel + ES group > MESGel group > Control group, which is consistent with that of H&E and Masson staining.

3. Conclusions

In summary, a new class of mechanically flexible, self-healable, and electroactive hydrogels (named MESGel) based on gelatin has been developed as a 3D e-skin scaffold for multi-functional motion sensing and acceleration of skin wound recovery combined with electrical stimulation. MESGel exhibited multifunctional properties including outstanding mechanical properties and flexibility, self-healing

characteristics, biodegradability, electroactivity, and biocompatibility. The high sensitivity and motion monitoring ability of the MESGel prospective the potential of hydrogel-based scaffolds and implantable medical devices. In addition, the MESGel exhibited a strong proreparative effect in a rat full-thickness skin defect model, and actively accelerated the *in vivo* wound recovery with wound area reduction, granulation tissue formation, collagen deposition enhancement, vascularization, and re-epithelialization. The elegant combination of electroactivity and bioelectronics in MESGel has been proven with promoted *in vitro* proliferation activity of the CHL cells. MESGel can be a promising candidate as not only a smart sensor for monitoring of human joint movement, but also an e-skin scaffold for wound healing. Furthermore, the combination of MESGel with electrical stimulation put a high-efficiency synergistic therapeutic strategy for the acceleration of wound repairing on track in the future, availing to the exploration of implantable and smart bioelectronics.

Data availability

All of the data reported in this work as available upon request.

CRediT authors statement

Ma**nhui Zheng**: Data curation, Writing-Original draft preparation; **Ouyang Yue**: Conceptualization, Methodology, Software; **Mengdi Hou**: Data curation, Methodology, Software; **Huijie Zhang**: Visualization, Investigation; **Sebastian Beyer**: Writing-Reviewing and Editing; **Anna Maria Blocki**: Writing-Reviewing and Editing; **Qin Wang**: Data curation, Methodology, Software; **Guidong Gong**: Methodology, Software; Supervision. **Xuechuan Wang**, **Xinhua Liu**, **Junling Guo**; **Xuechuan Wang**, **Xinhua Liu**, **Junling Guo**: Writing-Reviewing and Editing.

Declaration of competing interest

The authors declare that they have no known competing financial interests or personal relationships that could have appeared to influence the work reported in this paper.

Acknowledgements

We acknowledge the funding support of National Natural Science Foundation of China (21808133, 21804084), Science and Technology Project of Xianyang City (Grant 2018k02-28), The Fellowship of China Postdoctoral Science Foundation (2021M692000), and Basic Research Project of Wenzhou City (2019Y1073). The work in the J.G. laboratory was financially supported by the National Global Talents Recruitment Program (J.G.), State Key Laboratory of Polymer Materials Engineering (J.G., Grant No. Sklpme 2020-3-01), Double First Class University Plan (J.G.), Key Laboratory of Leather Chemistry and Engineering (J.G.), National Engineering Research Center of Clean Technology in Leather Industry (J.G.).

Appendix A. Supplementary data

Supplementary data to this article can be found online at https://doi.org/10.1016/j.biomaterials.2021.121026.

References

[1] H.R. Ashbee, E.G.V. Evans, Immunology of diseases associated with Malassezia species, Clin. Microbiol. Rev. 15 (1) (2002) 21–57.
[2] D.N. Herndon, R.E. Barrow, R.L. Rutan, T.C. Rutan, M.H. Desai, S. Abston, A comparison of conservative versus early excision. Therapies in severely burned patients, Ann. Surg. 209 (5) (1989) 547.
[3] K. Kalantari, E. Mostafavi, A.M. Afifi, Z. Izadiyan, H. Jahangirian, R. Rafiee-Moghaddam, T.J. Webster, Wound dressings functionalized with silver nanoparticles: promises and pitfalls, Nanoscale 12 (4) (2020) 2268–2291.
[4] S.P. Hernández Martínez, T.I. Rivera González, M.A. Franco Molina, J.J. Bollain y Goytia, J.J. Martínez Sanmiguel, D.G. Zárate Triviño, C. Rodríguez Padilla, A novel gold calreticulin nanocomposite based on chitosan for wound healing in a diabetic mice model, Nanomaterials 9 (1) (2019) 75.
[5] Y.H. Lu, Y.A. Wang, J.Y. Zhang, X.F. Hu, Z.Y. Yang, Y. Guo, Y.B. Wang, In-situ doping of a conductive hydrogel with low protein absorption and bacterial adhesion for electrical stimulation of chronic wounds, Acta Biomater. 89 (2019) 217–226.
[6] E. Calo, V.V. Khutoryanskiy, Biomedical applications of hydrogels: a review of patents and commercial products, Eur. Polym. J. 65 (2015) 252–267.
[7] N.K. Selvan, T.S. Shanmugarajan, V.N.V.A. Uppuluri, Hydrogel based scaffolding polymeric biomaterials: approaches towards skin tissue regeneration, J. Drug Deliv. Sci. Technol. 55 (2020) 101456.
[8] A.C. Daly, L. Riley, T. Segura, J.A. Burdick, Hydrogel microparticles for biomedical applications, Nat. Rev. Mater. 5 (1) (2020) 20–43.
[9] Q.T. Huang, Y.J. Zou, M.C. Arno, S. Chen, T. Wang, J.Y. Gao, A.P. Dove, J.Z. Du, Hydrogel scaffolds for differentiation of adipose-derived stem cells, Chem. Soc. Rev. 46 (20) (2017) 6255–6275.
[10] Y. Tu, N. Chen, C. Li, H. Liu, R. Zhu, S. Chen, Q. Xiao, J. Liu, S. Ramakrishna, L. He, Advances in injectable self-healing biomedical hydrogels, Acta Biomater. 90 (2019) 1–20.
[11] P.X. Ma, Biomimetic materials for tissue engineering, Adv. Drug Deliv. Rev. 60 (2) (2008) 184–198.
[12] Y. Tabata, Y. Ikada, Protein release from gelatin matrices, Adv. Drug Deliv. Rev. 31 (3) (1998) 287–301.
[13] K. Yue, T.D. Santiago, M.M. Alvarez, A. Tamayol, N. Annabi, A. Khademhosseini, Synthesis, properties, and biomedical applications of gelatin methacryloyl (GelMA) hydrogels, Biomaterials 73 (2015) 254–271.
[14] Y. Dong, S. A, M. Rodrigues, X. Li, S.H. Kwon, N. Kosaric, S. Khong, Y. Gao, W. Wang, G.C. Gurtner, Injectable and tunable gelatin hydrogels enhance stem cell retention and improve cutaneous wound healing, Adv. Funct. Mater. 27 (24) (2017) 1606619.
[15] M.E. 8Hoque, T. Nuge, K.Y. Tshai, N. Nordin, V. Prasad, Gelatin based scaffolds for tissue engineering – a review, Polym. Res. J. 9 (2015) 15–32.
[16] A. Sheikhi, J. De Rutte, R. Haghniaz, O. Akouissi, A. Sohrabi, D. Di Carlo, A. Khademhosseini, Microfluidic-enabled bottom-up hydrogels from annealable naturally-derived protein microbeads, Biomaterials 192 (2019) 560–568.
[17] S. Gnavi, L. di Blasio, C. Tonda-Turo, A. Mancardi, L. Primo, G. Ciardelli, G. Gambarotta, S. Geuna, I. Perroteau, Gelatin-based hydrogel for vascular endothelial growth factor release in peripheral nerve tissue engineering, J. Tissue Eng. Regener. Med. 11 (2) (2017) 459–470.
[18] M.H. Ho, D.M. Wang, H.J. Hsieh, H.C. Liu, T.Y. Hsien, J.Y. Lai, L.T. Hou, Preparation and characterization of RGD-immobilized chitosan scaffolds, Biomaterials 26 (16) (2005) 3197–3206.
[19] R. Yu, Y. Zhang, M. Barboiu, M. Maumus, D. Noel, C. Jorgensen, S.M. Li, Biobased pH-responsive and self-healing hydrogels prepared from O-carboxymethyl chitosan and a 3-dimensional dynamer as cartilage engineering scaffold, Carbohydr. Polym. 244 (2020) 116471.
[20] Y.J. Tu, N.A. Chen, C.P. Li, H.Q. Liu, R. Zhu, S.F. Chen, Q. Xiao, J.H. Liu, S. Ramakrishna, L.M. He, Advances in injectable self-healing biomedical hydrogels, Acta Biomater. 90 (2019) 1–20.
[21] J. Cameron, Electrical properties of tissue, in: F.A. Duck (Ed.), Physical Properties of Tissues, Academic Press, London, 1990, pp. 167–223.
[22] S. Young, S. Hampton, M. Tadej, Study to evaluate the effect of low-intensity pulsed electrical currents on levels of oedema in chronic non-healing wounds, J. Wound Care 20 (8) (2011) 368–370.
[23] J.Y. So, J. Lee, Y. Ahn, D. Kang, W. Jung, W.G. Bae, The synergistic effect of biomimetic electrical stimulation and extracellular-matrix-mimetic nanopattern for upregulating cell activities, Biosens. Bioelectron. 167 (2020) 112470.
[24] Y. Chen, Y. Liang, J. Liu, J.R. Yang, N.X. Jia, C.H. Zhu, J.P. Zhang, Optimizing microenvironment by integrating negative pressure and exogenous electric fields via a flexible porous conductive dressing to accelerate wound healing, Biomater. Sci. 9 (1) (2021) 238–251.
[25] R. Luo, J. Dai, J. Zhang, Z. Li, Accelerated skin wound healing by electrical stimulation, Adv. Healthcare Mater (2021) 2100557.
[26] A. Mohammed, A.-R. Teresa, B. Mohamed, B. Ardeshir, The efficacy of electrical stimulation in lower extremity cutaneous wound healing: a systematic review, Exp. Dermatol. 26 (2017) 171–178.
[27] A. Huttenlocher, A.R. Horwitz, Wound healing with electric potential, N. Engl. J. Med. 356 (3) (2007) 303–304.
[28] A. Datta, M. Elwassif, M. Bikson, Bio-heat transfer model of transcranial DC stimulation: comparison of conventional pad versus ring electrode, in: Annual International Conference of the IEEE Engineering in Medicine and Biology Society. IEEE Engineering in Medicine and Biology Society. Annual International Conference vol. 2009, 2009, pp. 670–673.
[29] A.N. Dalrymple, U.A. Robles, M. Huynh, B.A. Nayagam, R.A. Green, L.A. Poole-Warren, J.B. Fallon, R.K. Shepherd, Electrochemical and biological performance of chronically stimulated conductive hydrogel electrodes, J. Neural. Eng. 17 (2) (2020), 026018.
[30] J. Goding, A. Gilmour, P. Martens, L. Poole-Warren, R. Green, Interpenetrating conducting hydrogel materials for neural interfacing electrodes, Adv. Healthcare Mater. 6 (9) (2017) 1601177.
[31] S. Young, S. Hampton, M. Tadej, Study to evaluate the effect of low-intensity pulsed electrical currents on levels of oedema in chronic non-healing wounds, J. Wound Care 20 (2011) 368–373.

[32] S.W. Zhao, P. Tseng, J. Grasman, Y. Wang, W.Y. Li, B. Napier, B. Yavuz, Y. Chen, L. Howell, J. Rincon, F.G. Omenetto, D.L. Kaplan, Programmable hydrogel ionic circuits for biologically matched electronic interfaces, Adv. Mater. 30 (25) (2018) 1800598.
[33] B. Ferrigno, R. Bordett, N. Duraisamy, J. Moskow, M.R. Arul, S. Rudraiah, S. P. Nukavarapu, A.T. Vella, S.G. Kumbar, Bioactive polymeric materials and electrical stimulation strategies for musculoskeletal tissue repair and regeneration, Bioact. Mater. 5 (3) (2020) 468–485.
[34] S. Naskar, V. Kumaran, Y.S. Markandeya, B. Mehta, B. Basu, Neurogenesis-on-Chip: electric field modulated transdifferentiation of human mesenchymal stem cell and mouse muscle precursor cell coculture, Biomaterials 226 (2020) 119522.
[35] S. Li, D. Lu, J. Tang, J. Min, M. Hu, Y. Li, Y. Liu, L. Wang, C. Liu, L. Hong, Electrical stimulation activates fibroblasts through the elevation of intracellular free Ca^{2+}: potential mechanism of pelvic electrical stimulation therapy, BioMed Res. Int. 2019 (2019) 7387803.
[36] H. Kai, T. Yamauchi, Y. Ogawa, A. Tsubota, T. Magome, T. Miyake, K. Yamasaki, M. Nishizawa, Accelerated wound healing on skin by electrical stimulation with a bioelectric plaster, Adv. Healthcare Mater. 6 (22) (2017) 1700465.
[37] S.I. Reger, A. Hyodo, S. Negami, H.E. Kambic, V. Sahgal, Experimental wound healing with electrical stimulation, Artif. Organs 23 (5) (1999) 460–462.
[38] Z.X. Deng, Y. Guo, X. Zhao, L.C. Li, R.N. Dong, B.L. Guo, P.X. Ma, Stretchable degradable and electroactive shape memory copolymers with tunable recovery temperature enhance myogenic differentiation, Acta Biomater. 46 (2016) 234–244.
[39] Y.B. Wu, L. Wang, B.L. Guo, Y.P. Shao, P.X. Ma, Electroactive biodegradable polyurethane significantly enhanced Schwann cells myelin gene expression and neurotrophin secretion for peripheral nerve tissue engineering, Biomaterials 87 (2016) 18–31.
[40] F. Ershad, A. Thukral, J. Yue, P. Comeaux, Y. Lu, H. Shim, K. Sim, N.-I. Kim, Z. Rao, R. Guevara, Ultra-conformal drawn-on-skin electronics for multifunctional motion artifact-free sensing and point-of-care treatment, Nat. Commun. 11 (1) (2020) 1–13.
[41] Y. Zhao, Z. Li, S. Song, K. Yang, H. Liu, Z. Yang, J. Wang, B. Yang, Q. Lin, Skin-inspired antibacterial conductive hydrogels for epidermal sensors and diabetic foot wound dressings, Adv. Funct. Mater. 29 (31) (2019) 1901474.
[42] M. Talikowska, X.X. Fu, G. Lisak, Application of conducting polymers to wound care and skin tissue engineering: a review, Biosens. Bioelectron. 135 (2019) 50–63.
[43] M. Rouabhia, H.J. Park, A. Abedin-Do, Y. Douville, M. Méthot, Z. Zhang, Electrical stimulation promotes the proliferation of human keratinocytes, increases the production of keratin 5 and 14, and increases the phosphorylation of ERK1/2 and p38 MAP kinases, J. Tissue Eng. Regen. Med. 14 (7) (2020) 909–919.
[44] Z. Yahong, L. Yunyun, D. Supeng, Z. Kunyu, M. Hai-Quan, Y. Yumin, Application of conductive PPy/SF composite scaffold and electrical stimulation for neural tissue engineering, Biomaterials 255 (2020) 120164.
[45] F. Zhiyuan, D. Junjie, Y.L. Peter, R.C. Daphney, S. Yunfei, Z. Pu, K. Taku, P. B. Elizabeth, H. Lin, C. Hao, A new class of biological materials: cell membrane-derived hydrogel scaffolds, Biomaterials 197 (2019) 244–254.
[46] R. Sarvari, B. Massoumi, A. Zareh, Y. Beygi-Khosrowshahi, S. Agbolaghi, Porous conductive and biocompatible scaffolds on the basis of polycaprolactone and polythiophene for scaffolding, Polym. Bull. 77 (4) (2020) 1829–1846.
[47] F. Hempel, J.K.Y. Law, T.C. Nguyen, W. Munief, X.L. Lu, V. Pachauri, A. Susloparova, X.T. Vu, S. Ingebrandt, PEDOT:PSS organic electrochemical transistor arrays for extracellular electrophysiological sensing of cardiac cells, Biosens. Bioelectron. 93 (2017) 132–138.
[48] J.H. Kim, S.M. Kim, G. Kim, M.H. Yoon, Designing polymeric mixed conductors and their application to electrochemical-transistor-based biosensors, Macromol. Biosci. 20 (11) (2020) 2000211.
[49] A.G. Guex, J.L. Puetzer, A. Armgarth, E. Littmann, E. Stavrinidou, E.P. Giannelis, G.G. Malliaras, M.M. Stevens, Highly porous scaffolds of PEDOT:PSS for bone tissue engineering, Acta Biomater. 62 (2017) 91–101.
[50] S. Stritesky, A. Markova, J. Vitecek, E. Safarikova, M. Hrabal, L. Kubac, L. Kubala, M. Weiter, M. Vala, Printing inks of electroactive polymer PEDOT:PSS: the study of biocompatibility, stability, and electrical properties, J. Biomed. Mater. Res. 106 (4) (2018) 1121–1128.
[51] A.R. Spencer, A. Primbetova, A.N. Koppes, R.A. Koppes, H. Fenniri, N. Annabi, Electroconductive gelatin methacryloyl-PEDOT:PSS composite hydrogels: design, synthesis, and properties, ACS Biomater. Sci. Eng. 4 (5) (2018) 1558–1567.
[52] J.W. Nichol, S.T. Koshy, H. Bae, C.M. Hwang, S. Yamanlar, A. Khademhosseini, Cell-laden microengineered gelatin methacrylate hydrogels, Biomaterials 31 (21) (2010) 5536–5544.
[53] L. Ouyang, Y. Dan, Z. Shao, S. Yang, C. Yang, G. Liu, D. Duan, MMP-sensitive PEG hydrogel modified with RGD promotes bFGF, VEGF and EPC-mediated angiogenesis, Exp. Ther. Med. 18 (4) (2019) 2933–2941.
[54] S. Burattini, B.W. Greenland, D.H. Merino, W. Weng, J. Seppala, H.M. Colquhoun, W. Hayes, M.E. Mackay, I.W. Hamley, S.J. Rowan, A healable supramolecular polymer blend based on aromatic $\pi-\pi$ stacking and hydrogen-bonding interactions, J. Am. Chem. Soc. 132 (34) (2010) 12051–12058.
[55] L. Cai, S. Liu, J. Guo, Y. Jia, Polypeptide-based self-healing hydrogels: design and biomedical applications, Acta Biomater. 113 (2020) 84–100.
[56] B. Gyarmati, B.Á. Szilágyi, A. Szilágyi, Reversible interactions in self-healing and shape memory hydrogels, Eur. Polym. J. 93 (2017) 642–669.
[57] X. Ji, Z. Li, Y. Hu, H. Xie, W. Wu, F. Song, H. Liu, J. Wang, M. Jiang, J.W.Y. Lam, B. Z. Tang, Bioinspired hydrogels with muscle-like structure for AIEgen-guided selective self-healing, CCS Chem 3 (4) (2021) 1146–1156.
[58] X.H. Liu, M.H. Zheng, X.C. Wang, X.M. Luo, M.D. Hou, O. Yue, Biofabrication and characterization of collagens with different hierarchical architectures, ACS Biomater. Sci. Eng. 6 (1) (2020) 739–748.
[59] Y.H. Zhao, Y.Y. Liang, S.P. Ding, K.Y. Zhang, H.Q. Mao, Y.M. Yang, Application of conductive PPy/SF composite scaffold and electrical stimulation for neural tissue engineering, Biomaterials 255 (2020) 120164.